Journal of Medicinal Chemistry

ARTICLE

pubs.acs.org/jmc

Covalent Inhibitors of Fatty Acid Amide Hydrolase: A Rationale for the Activity of Piperidine and Piperazine Aryl Ureas

Giulia Palermo,[†] Davide Branduardi,[†] Matteo Masetti,[†,‡] Alessio Lodola,[§] Marco Mor,[§] Daniele Piomelli,[†,∥] Andrea Cavalli,[*,†,‡] and Marco De Vivo[*,†]

[†]Department of Drug Discovery and Development, Istituto Italiano di Tecnologia, Via Morego 30, 16163 Genova, Italy

[‡]Department of Pharmaceutical Sciences, University of Bologna, via Belmeloro 6, I-40126 Bologna, Italy

[§]Dipartimento Farmaceutico, Università degli Studi di Parma, Viale G. P. Usberti 27/A Campus Universitario, I-43100 Parma, Italy

[∥]Department of Pharmacology, University of California, Irvine, California 92697, United States

Supporting Information

ABSTRACT: Recently, covalent drugs have attracted great interest in the drug discovery community, with successful examples that have demonstrated their therapeutic effects. Here, we focus on the covalent inhibition of the fatty acid amide hydrolase (FAAH), which is a promising strategy in the treatment of pain and inflammation. Among the most recent and potent FAAH inhibitors (FAAH*i*), there are the cyclic piperidine and piperazine aryl ureas. FAAH hydrolyzes efficiently the amide bond of these compounds, forming a covalent enzyme−inhibitor adduct. To rationalize this experimental evidence, we performed an extensive computational analysis centered on piperidine-based PF750 (**1**) and piperazine-based JNJ1661010 (**2**), two potent lead compounds used to generate covalent inhibitors as clinical candidates. We found that FAAH induces a distortion of the amide bond of the piperidine and piperazine aryl ureas. Quantum mechanics/molecular mechanics $\Delta E_{LUMO-HOMO}$ energies indicate that the observed enzyme-induced distortion of the amide bond favors the formation of a covalent FAAH−inhibitor adduct. These findings could help in the rational structure-based design of novel covalent FAAH*i*.

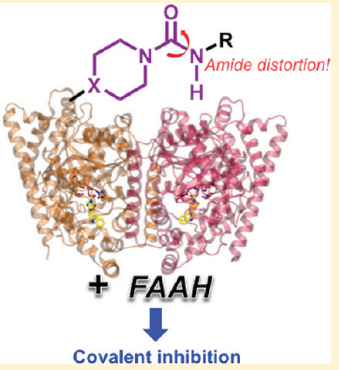

INTRODUCTION

The drug discovery community is looking at covalent drugs with a renewed interest.[1] Indeed, covalent drugs have been approved for several clinical indications and have had a major positive impact on human health.[2] In this scenario, fatty acid amide hydrolase (FAAH) represents a promising target for the discovery of covalent drugs for the treatment of pain, inflammation, and other diseases.[3] FAAH is an integral membrane protein belonging to the amidase signature family of enzymes (Figure 1),[4] and it is responsible for the deactivating hydrolysis of several endogenous fatty acid amides such as anandamide (AEA), palmitoylethanolamide (PEA), and oleoylethanolamide.[5] Therefore, the inhibition of FAAH can be used to modulate the level of endogenous fatty acid ethanolamides,[6] which in turn has been proven to induce anti-inflammatory, antidepressant, analgesic, and anxiolytic effects.[7] In addition, these actions occur in the absence of changes in motility, sleep, and weight gain or other side effects typically observed with direct CB1 agonists.[8]

FAAH is a serine hydrolase characterized by an unusual Ser-Ser-Lys catalytic triad (Ser241-Ser217-Lys142) that cleaves amides and esters with similar rates.[9] Over the past few years, a number of crystal structures of FAAH bound to covalent inhibitors have been resolved.[10] This experimental evidence, coupled with computational studies,[11] has elucidated the enzymatic mechanism of FAAH. First, substrate hydrolysis is initiated by activation of the nucleophile Ser241. This occurs through a proton transfer event that leads the side chain proton of Ser241 to Lys142, shuttled via Ser217. Then, the activated Ser241 attacks the carbonyl group of the substrate, leading to the formation of a tetrahedral intermediate. Finally, the protonation of the leaving group by Lys142, through a proton shuttle that again involves Ser217, facilitates the leaving group departure and formation of the acylated enzyme (Scheme 1a).

Several classes of FAAH inhibitors[12] (FAAH*i*) react and form a covalent bond with Ser241. Among these molecules are potent electrophilic compounds characterized by the presence of an activated carbonyl group. These include trifluoromethyl ketones, α-keto esters, α-keto amides, and α-ketoheterocycles, such as OL-135. However, most of these compounds have low target selectivity and limited efficacy in vivo.[12]

A class of FAAH*i* with a promising druglike profile consists of potent and irreversible FAAH*i* based on an *N*-cyclohexylcarbamic acid *O*-aryl ester template, including URB524 (IC_{50} = 63 nM).[8a,13] Optimization of URB524 led to URB597 (the 3′-$CONH_2$ derivative of URB524),[14] a highly potent FAAH*i* in vitro (IC_{50} = 4.6 nM) and in vivo (ED_{50} = 0.15 mg/kg, in rat).[8a,15] Interestingly, a brain-impenetrant member of this class of compounds

Received: April 14, 2011
Published: August 11, 2011

was recently disclosed [URB937 (IC_{50} = 26.8 ± 4.9 nM)] and shown to produce substantial analgesic effects in animal models, which is suggestive that inhibition of peripheral FAAH activity might represent a novel approach for the treatment of pain.[16]

The unique ability of FAAH to cleave amides and esters at similar rates suggests, however, that not only carbamates but also ureas could act as good carbamoylating agents. Even though the substitution of the carbamate functionality with an acyclic urea led to mostly inactive compounds,[13,17] cyclic piperidine- and piperazine-based molecules were identified by Pfizer and Cravatt's lab as a novel class of potent FAAH*i*.[18] Among them is the irreversible *N*-phenyl-4-(quinolin-3-ylmethyl)piperidine-1-carboxamide (PF750, **1**) (IC_{50} = 16.2 nM)[18] and the reversible piperazine-based *N*-phenyl-4-(3-phenyl-1,2,4-thiadiazol-5-yl)-1-piperazine-carboxamide (JNJ1661010, **2**) (IC_{50} = 33 ± 2.1 nM).[19]

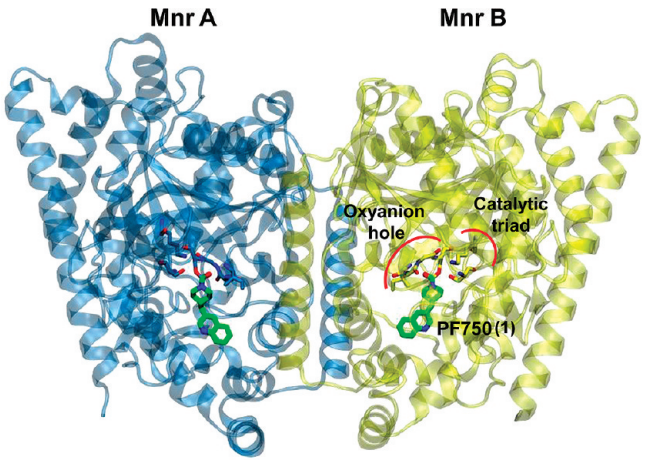

Figure 1. X-ray structure of the (*h*/*r*) FAAH protein in complex with the PF750 inhibitor (Protein Data Bank entry 2VYA).[10b] The FAAH protein consists of two monomers: Mnr A is represented with blue ribbons, and Mnr B is colored yellow. The catalytic triad (Ser241-Ser217-Lys142) and oxyanion hole (Ile238, Gly239, and Gly240) residues are colored blue (Mnr A) and shown as yellow sticks (Mnr B). PF750 is shown as green sticks.

The piperidine or piperazine moiety of these compounds seems to favor, somehow, the covalent interaction of the inhibitor with Ser241. In this respect, Cravatt and co-workers have proposed that the limited flexibility of piperidine- and piperazine-based inhibitors could favor the conformational distortion of their urea functionality at the FAAH active site, favoring the formation of a covalent bond between the inhibitor and Ser241 (Scheme 1).[18] This hypothesis, however, has not been investigated yet, and the mechanism of piperidine and piperazine FAAH*i* remains poorly understood at the atomic level.

Here, we report on a comparative study based on molecular dynamics (MD) simulations and quantum mechanics/molecular mechanics (QM/MM) computations that aims to characterize the difference between cyclic and inactive acyclic ureas. Three structurally different compounds were considered: the two potent lead compounds piperidine-based **1** and piperazine-based **2**, along with an inactive acyclic 1-cyclohexyl-3-naphthalen-2-ylurea, here termed Cpd3 (**3**) (IC_{50} < 30000 nM) (Figure 2).[13] We have characterized the conformational flexibility of these compounds in water and in complex with FAAH. Our results support the hypothesis[18] that FAAH is able to induce a distortion of the amide bond of the piperidine and piperazine compounds. The twist of the amide bond likely facilitates the amide bond hydrolysis and formation of the covalent inhibitor−enzyme adduct.[20] On the other hand, the rigidity of the planar urea moiety in the acyclic derivative seems to prevent its good fit into the catalytic site, which might partially explain its lack of inhibitory activity.

COMPUTATIONAL MATERIALS AND METHODS

Structural Models. Three model systems formed by FAAH in complex with either **1** or **2** and with the inactive derivative **3** were considered for calculations (see Figures 1 and 2). All model systems were based on the crystallographic structure of the humanized rat FAAH protein [(*h*/*r*) FAAH] in complex with **1**, determined at 2.75 Å resolution (Protein Data Bank entry 2VYA).[10b] The X-ray structure of the FAAH·**1** complex consists of monomer A (Mnr A) and monomer B (Mnr B) formed by 574 residues in total, one Cl^- ion, 84 cocrystallized water molecules, and two **1** residues (one per monomer) covalently attached to

Scheme 1. (a) Mechanism of Substrate Hydrolysis by FAAH (shown for a generic amide substrate) and (b) Proposed Mechanism of FAAH Inhibition by the Piperidine and Piperazine Ureas (shown for 1[18])[a]

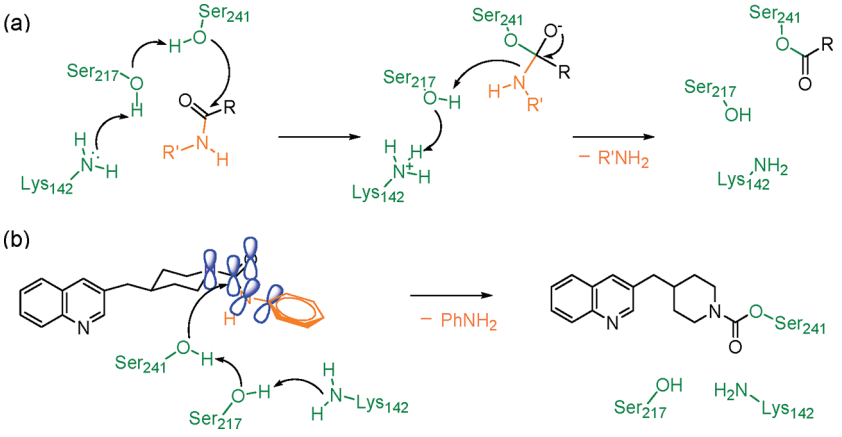

[a] FAAH residues are colored green, and the leaving group is colored orange. The enzyme-induced conformational change in the piperidine and piperazine urea weakens the conjugation of the nitrogen lone pair with the carbonyl and allows the nucleophilic attack by Ser241. This leads to a covalent enzyme−inhibitor adduct.

dx.doi.org/10.1021/jm2004283 |*J. Med. Chem.* 2011, 54, 6612–6623

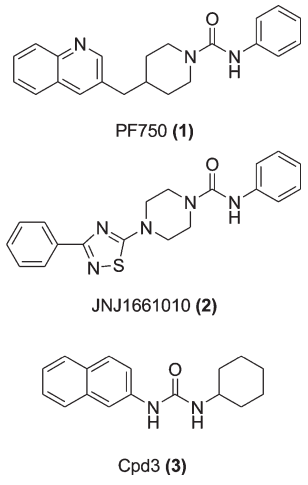

Figure 2. Piperidine urea **1** (IC_{50} = 16.2 nM),[18] piperazine urea **2** (IC_{50} = 33 ± 2.1 nM),[19] and acyclic urea **3** (IC_{50} < 30000 nM).[13]

Ser241 of FAAH through a carbamate bond. Importantly, this structure contains active site residues of the human protein, within the parent rat protein, including the key residues of the catalytic triad (Ser241-Ser217-Lys142) and those of the oxyanion hole (Ile238, Gly239, Gly240, and Ser241). The binding mode of **1** was constructed by adding the leaving group to the crystallographic pose. The piperazinic **2** binding pose was generated via computational docking of the ligand to the FAAH binding site. Docking calculations were conducted using Autodock 4.2[21] (see the Supporting Information). The final docked structure of **2** is in agreement with its binding pose proposed by Keith et al.[19] The comparison between the binding mode of the cocrystallized ligand **1** and the docked **2** compound shows that the urea occupies the same region of the pocket (see the Supporting Information). Because of the structural similarity between **1** and **3**, the binding pose of the latter was modeled by manually modifying **1** within the binding site (see the Supporting Information).

Molecular Dynamics (MD) Simulations. A standard MD setup was adopted for all three complexes, namely, FAAH·**1**, FAAH·**2**, and FAAH·**3**. Hydrogen atoms were added assuming standard bond lengths and angles. The simulations were performed with deprotonated Lys142, as proposed for the catalytic mechanism of FAAH.[10a] Each of the three complexes was immersed in a rectangular TIP3P water box.[22] The starting size of the solvated system was approximately 100 Å × 100 Å × 125 Å for all three complexes, containing ~36550 water molecules and a total of ~126500 atoms. The charge of the systems was neutralized by adding an exact number of counterions (eight Cl^- ions were added in each model) whose optimal positions were located using the xLEAP program of the AMBER10 package.[23] The AMBER99SB force field[24] was adopted for the protein. Ligands **1**−**3** were treated with the General Amber Force Field[25] together with ad hoc charges calculated following the RESP procedure (see the Supporting Information).[26] The SHAKE[27] algorithm was used for all the covalent bonds that contain an H atom, thus allowing a time step of 2 fs for the integration of the equations of motion. All the simulations were performed by using the NAMD 2.7 package.[28] Periodic boundary conditions were applied, and the particle mesh Ewald method was used to evaluate long-range electrostatic interactions with a direct cutoff of 10 Å. All the simulations were conducted with the following protocol. First, the systems were optimized and thermalized to 300 K in the NVT ensemble using a Langevin bath,[29] in three consecutive steps. (1) The solvent was first equilibrated, slowly increasing the temperature from 0 to 100 K and keeping the protein fixed. (2) The temperature was further increased to 200 K while only the coordinates of backbone atoms of the protein were kept fixed. (3) Constraints were released and the systems simulated to reach a temperature of 300 K. Subsequently, MD for 100 ns was performed for each system in the NPT ensemble under standard conditions using a Langevin piston. Coordinates of the systems were collected every 2 ps, for a total of ~50000 frames for each run. Statistics was accumulated during the last 98 ns of each run. The structural analysis here reported was obtained using data from the two FAAH monomers that form each complex, considered as independent, for a total of ~100000 structures.

Scheme 2. Descriptors Used for the Analysis of the Amide Bond Distortion[a]

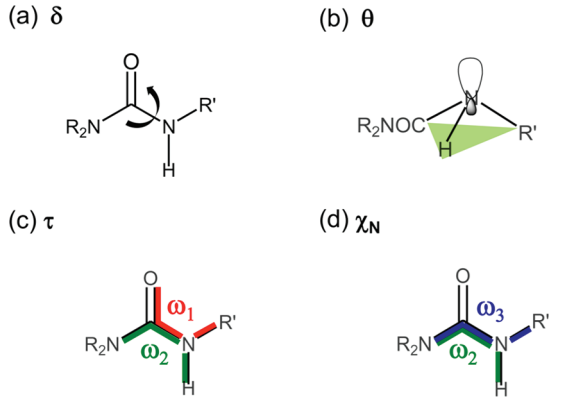

[a] (a) Dihedral angle δ is the $R_2N-C-N-H$ angle. (b) Improper torsion θ centered on the secondary amine nitrogen. (c) Mean twisting angle $\tau = (\omega_1 + \omega_2)/2$. (d) $\chi_N = \omega_2 - \omega_3 + \pi(\mathrm{mod}\ 2\pi)$.[30b]

Unbound Systems. Compounds **1**−**3** were also simulated via classical MD in a pure water box. **1** was immersed in a 43.1 Å × 31.0 Å × 29.4 Å box, with 1314 water molecules and 3991 atoms. Piperazine **2** was immersed in a 43.3 Å × 31.3 Å × 29.8 Å box of 1348 water molecules, for a total of 4089 atoms. The water box for acyclic **3** was 40.3 Å × 33.7 Å × 29.2 Å, including 1202 water molecules and 3646 atoms. The same protocol described above was adopted for optimization and thermalization.

Analysis of Structural Data. The amide bond distortion was characterized by analyzing the following structural parameters: (1) the $R_2N-C-N-H$ dihedral angle [termed δ (Scheme 2a)] and (2) the improper torsion centered on the secondary amine nitrogen [termed θ (Scheme 2b)].

For completeness, the planarity of the amino group was also analyzed using the internal coordinates τ (eq 1) and χ_N (eq 2), originally defined by Dunitz.[30] The τ and χ_N parameters are functions of the torsion angles defined by the amide C−N bond, as follows:

$$\tau = (\omega_1 + \omega_2)/2 \quad (1)$$

$$\chi_N = \omega_2 - \omega_3 + \pi(\mathrm{mod}\ 2\pi) \quad (2)$$

where ω_1 is the $O{=}C-N-R'$ angle, ω_2 is the $R_2N-C-N-H$ angle, and ω_3 is the $R_2N-C-N-R'$ angle (Scheme 2). τ is a measure of the mean twisting angle between the C−N bond and ranges from 0° (planar amide group) to 90° (when the $O{=}C-NR_2$ and $R'-N-H$ planes are perpendicular). The χ_N parameter determines the degree of pyramidalization at the N atom, and it may take values between approximately 0° (planar sp^2 geometry) and 60° (tetrahedral sp^3 geometry). The geometrical meaning of τ and χ_N is shown in Scheme 2. We consider here the absolute values for these angles reported on the 0−90° quadrant.

Quantum Mechanics/Molecular Mechanics Calculations. QM/MM calculations were performed to obtain the HOMO−LUMO energy gap ($\Delta E_{LUMO-HOMO}$) of the reactive complex formed by inhibitors **1** and **2** and the enzyme. Because **3** is neither experimentally active nor stable during the simulations, it was not considered for these calculations. Calculations were conducted using the two-layer ONIOM

dx.doi.org/10.1021/jm2004283 |J. Med. Chem. 2011, 54, 6612–6623

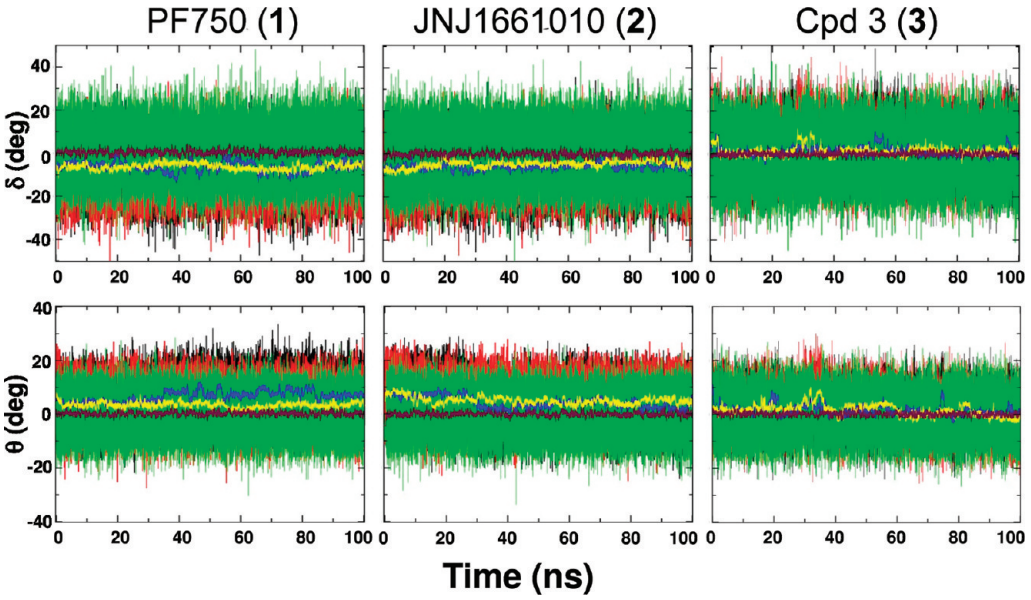

Figure 3. Dihedral angle δ (top) and improper torsion θ (bottom w) value fluctuation during the 100 ns MD simulation of **1** (left), **2** (middle), and **3** (right). Black and red thin lines are instantaneous values in Mnr A and Mnr B, respectively, while green thin lines are those in water. The running average values are calculated over 200 ps for δ and θ (blue and yellow thick lines for Mnr A and Mnr B, respectively). The maroon thick line represents the average value measured in water.

method,[31] as implemented in Gaussian09.[32] This approach allows treatment of the system at different levels of theory. The entire system (real) is computed with a low level of theory (MM), while the inner layer (model) is treated at a high level of theory (QM). The expression of the ONIOM energy, E_{ONIOM}, is given via a subtractive QM/MM scheme:

$$E_{ONIOM} = E_{(high,model)} + E_{(low,real)} - E_{(low,model)} \quad (3)$$

The electrostatic interaction between the two layers was taken into account via electrostatic embedding.[33]

For the structures extracted from each of the MD runs, we built a QM/MM subsystem by retaining the ligand and the 79 residues that were within 8 Å of the ligand. The QM region consisted of the ligand and the following residues of the FAAH active site: the catalytic triad and oxyanion hole residues Ile238, Gly239, Gly240, and Met191, Phe192, and Asp237. The N- and C-termini of the residues were capped with the standard Ace (acetyl) and Nme (*N*-methyl) residues parametrized with the Amber force field.[24] A total number of 1525 and 1521 atoms were considered in the QM/MM calculations of the FAAH·**1** and FAAH·**2** complexes, respectively (complete list available as Supporting Information). The QM part resulted in 178 atoms for the FAAH·**1** system and 174 atoms for the FAAH·**2** system. The remaining part of the systems was treated with the AMBER99SB force field.[24] As a result, 500 snapshots were used to calculate $\Delta E_{LUMO-HOMO}$ by means of single-point energy calculations at the ONIOM (HF/6-311G**:Amber) level of theory, which was shown to give a good description of the orbital energies.[34]

In detail, we first calculated the $\Delta E_{LUMO-HOMO}$ values for 50 structural snapshots equally distributed over the δ range (−40° to 35°). These calculations were performed for both FAAH·**1** and FAAH·**2** complexes, for a total of 100 structures. Additionally, to better address the difference between the most distorted and planar structures, the average $\Delta E_{LUMO-HOMO}$ was determined using 100 structural snapshots randomly extracted within a range of 3° centered on the most populated state of δ and θ conformers of both complexes, for a total of 200 additional systems that showed the twist of the amide bond as detected during the dynamics. Namely, for the FAAH·**1** complex, configurations were selected within the following ranges: $-7° < \delta < -4°$, and $4° < \theta < 7°$. In the case of the FAAH·**2** complex, the selected states were taken in the following ranges: $-8° < \delta < -5°$, and $4° < \theta < 7°$ (see Scheme 2 and Figures 3 and 4). For comparison, the average $\Delta E_{LUMO-HOMO}$ was also calculated for the less populated configurations characterized by the planarity of the ligand amide bond (δ and θ around ∼0°). Also in this case, a set of structures from classical MD simulations of both FAAH·**1** and FAAH·**2** complexes were collected within a 3° window, for a total of 200 additional model systems.

RESULTS

MD Simulations. *(h/r) FAAH·PF750 (**1**) Complex.* During the NPT run, the structural stability was evaluated by calculating the root-mean-square deviation (rmsd) with respect to the minimized X-ray structure. After a transient period of ∼2 ns, the rmsd for the all atoms of the protein settled at 2.42 ± 0.16 Å, while the rmsd for the heavy atoms was ∼1.56 ± 0.20 Å. The rmsd of ligand **1** remained below ∼2 Å, while the **1** binding group (i.e., piperidine urea group) was very stable (rmsd of the N_2−C═O plane, 0.04 Å).

The **1** binding pose closely resembles that proposed by Mileni et al.[10b] The carbonyl carbon of the ligand remained in the proximity of Ser241 (C−O distance), at 2.95 ± 0.12 Å. Also, the H-bond pattern formed by the Ser241-Ser217-Lys142 catalytic triad was very stable; the distance between the side chain nitrogen of Lys142 and the hydroxyl oxygen of Ser217 was ∼1.83 ± 0.27 Å, while the length of the Ser217-Ser241 H-bond was 2.04 ± 0.23 Å. Throughout the simulations, **1** conserved an ordered H-bond network with the oxyanion hole residues (Ser241, Gly240, Gly239, and Ile238) and the main chain carbonyl oxygen of Met191. Overall, we found that the main interactions between FAAH and **1** were conserved during the simulations, which further evidenced the structural stability of the complex (see the Supporting Information for details).

dx.doi.org/10.1021/jm2004283 |*J. Med. Chem.* 2011, 54, 6612–6623

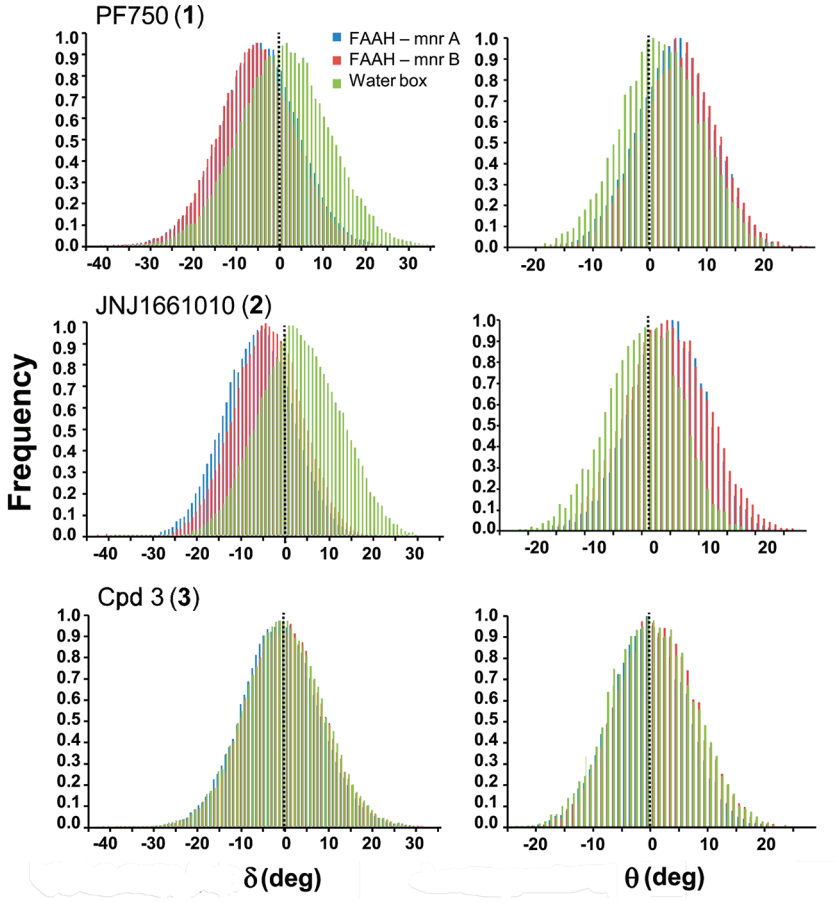

Figure 4. Probability distributions of the δ (left) and θ (right) angles shown for **1** (top), **2** (middle), and **3** (bottom) in complex with FAAH and in water. The δ and θ frequency distributions are indicated with blue and red colors for the selected compounds bound to FAAH Mnr A and FAAH Mnr B, respectively. The δ and θ distributions in water are colored green. The population of the δ and θ angles was evaluated by using a bin size of 1°.

Amide Bond in ***1***. During the simulations, **1** underwent small conformational changes within the FAAH binding site that involved primarily the piperidine moiety and a moderate twist of the hydrolytic amide bond. This evidence prompted us to compare the conformational flexibility of **1** within the enzyme with that in solution. We focused on the geometrical distortion of the amide bond during the simulations in terms of the distribution of dihedral angle δ and improper torsion θ, as described in Computational Materials and Methods. The time evolution of δ and θ during the MD is shown in Figure 3. There was a significant difference between the structural features of **1** within the enzyme and in solution. The average δ value within FAAH was equal to $-6.35 \pm 0.03°$ (standard error of the mean), while the average δ was $0.41 \pm 0.03°$ when simulated in a water box. The θ values confirmed the out-of-plane deformation of **1**'s urea functionality within the enzyme. Indeed, the average θ value was equal to $5.00 \pm 0.02°$ in complex with FAAH and $0.21 \pm 0.02°$ in solution.

The probability distributions of angles δ and θ along the MD simulations are reported in Figure 4. The population of **1**'s conformers in FAAH was centered on a δ value of approximately $-5°$, while in solution, δ was $\sim 0°$, showing that the planarity of the C−N bond in water is strongly influenced by the enzymatic environment. Accordingly, the distribution curve of the θ angle of the inhibitor was centered on $\theta \sim 6°$ when simulated in complex with FAAH, while θ was $\sim 0°$ when simulated in solution (see Table 1).

Table 1. Averages over the Last ~98 ns of MD Simulation for Inhibitor 1 within FAAH and in Water[a]

	δ	θ	τ	χ_N
Mnr A	-6.42 ± 0.03	6.63 ± 0.03	13.01 ± 0.03	23.15 ± 0.05
Mnr B	-6.29 ± 0.03	3.38 ± 0.02	11.01 ± 0.03	22.34 ± 0.05
FAAH	-6.35 ± 0.03	5.00 ± 0.02	12.01 ± 0.02	22.75 ± 0.04
water box	0.41 ± 0.04	0.21 ± 0.02	8.51 ± 0.02	16.81 ± 0.04

[a] δ is the $R_2N-C-N-H$ dihedral angle. θ is the improper torsion centered on the secondary amine nitrogen. τ is the mean twisting angle between the C−N bond. χ_N is the out-of-plane bending angle, a measure of the degree of pyramidalization at the N atom. The standard errors of the mean are reported. Angles are expressed in degrees.

For completeness, we here describe the amide bond distortion during dynamics according to the Dunitz internal coordinates τ and χ_N (Figure 5),[30b] as well. The average twist angle τ was $12.01 \pm 0.02°$ in FAAH and $8.51 \pm 0.02°$ in water, while the pyramidalization at the nitrogen, χ_N, was equal to $22.75 \pm 0.04°$ in FAAH and $16.81 \pm 0.04°$ in solution. Overall, these data further indicate the evident distortion of the hydrolytic amide bond of **1** when it is in complex with FAAH.

*(h/r) FAAH·JNJ1661010 (**2**) Complex.* After the equilibration, during the ~100 ns, the rmsd of the overall FAAH protein atoms oscillated around 2.38 ± 0.13 Å. The fluctuation of the protein

dx.doi.org/10.1021/jm2004283 |J. Med. Chem. 2011, 54, 6612–6623

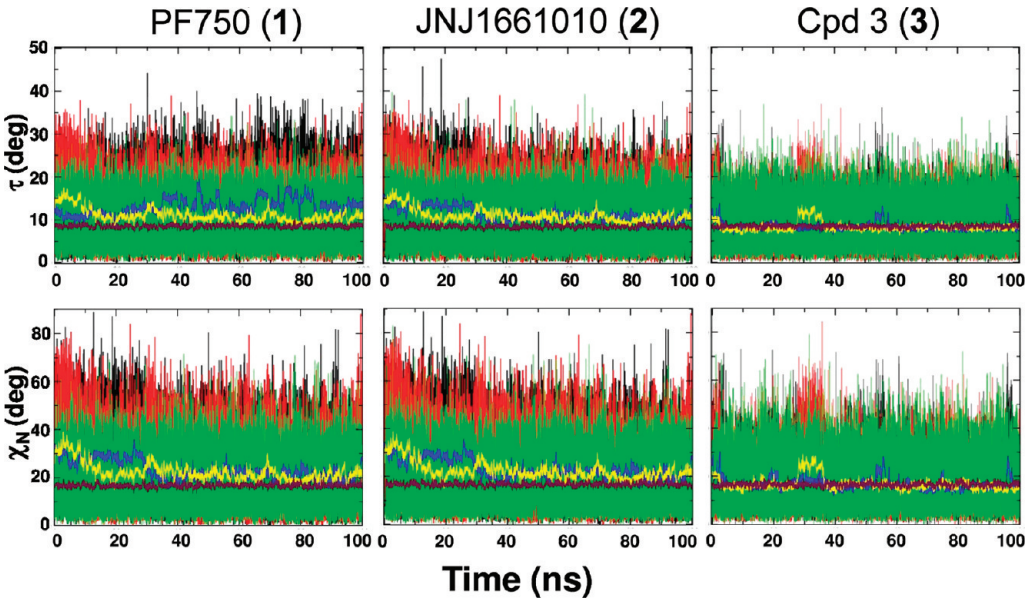

Figure 5. Twisting angle τ (top) and out-of-plane bending angle χ_N (bottom) value fluctuation during the 100 ns of MD simulation by **1** (left), **2** (middle), and **3** (right). Black and red thin lines denote instantaneous values in Mnr A and Mnr B, respectively, while green thin lines show those in water. The running average values are calculated over 200 ps for τ and χ_N (blue and yellow thick lines for Mnr A and Mnr B, respectively). The average τ and χ_N angles in water are colored maroon.

heavy atoms confirmed that the FAAH conformation remained consistently stable throughout the simulations (rmsd = 1.49 ± 0.18 Å). The rmsd of **2** was approximately 0.5−1 Å, while the urea functional group was highly stable (rmsd of the N_2−C═O plane, 0.04 ± 0.01 Å).

The key binding distances were well conserved in the ligand·protein complex. The C−O distance remained 2.90 ± 0.11 Å. The H-bond network of the catalytic triad was also well conserved: the Ser241−Ser217 average distance was 1.98 ± 0.20 Å, and the Ser217−Lys142 H-bond distance oscillated around ∼1.80 ± 0.11 Å. The interactions between the carbonyl oxygen of **2** and the NH groups of the FAAH oxyanion hole were very stable, as well as the H-bond between the aniline hydrogen of **2** and the main chain carbonyl oxygen of Met191. Key binding distances are reported in the Supporting Information. It is worth noting that **2** and **1** showed an analogous network of binding interactions. Indeed, the orientation within the FAAH active site of piperazine **2** is similar to the experimental pose of the cocrystallized piperidine FAAH*i* **1**[10b] and PF3845.[10c] Both compounds **1** and **2** place the heterocyclic moiety in the FAAH acyl chain binding channel, while the leaving group occupies the site of cytoplasmic access of the FAAH active site. This binding orientation of the cyclic urea-based FAAH*i* has been recently explored by Pfizer and Cravatt's lab through the modeling of benzothiophene piperidine and piperazine ureas as FAAH*i*.[35] Their results resemble the existing crystallographic data and further support the proposed mechanism of FAAH inhibition.[18]

Amide Bond in ***2***. As for **1**, the amide bond of **2** showed a distorted geometry when simulated in complex with FAAH. The average δ and θ values within FAAH were −5.22 ± 0.03° and 4.61 ± 0.02°, respectively. These values differ from those obtained in solution, where the amide bond remained planar (δ = −0.05 ± 0.03°, and θ = −0.01 ± 0.02°). Values of δ and θ during the dynamics are shown in Figure 3.

Table 2. Average over the Last ∼98 ns of MD Simulation for Inhibitor 2 within FAAH and in Water[a]

	δ	θ	τ	χ_N
Mnr A	−5.87 ± 0.03	4.24 ± 0.03	11.32 ± 0.03	23.15 ± 0.05
Mnr B	−4.57 ± 0.03	4.97 ± 0.02	11.01 ± 0.02	22.35 ± 0.05
FAAH	−5.22 ± 0.03	4.61 ± 0.02	11.16 ± 0.02	22.74 ± 0.04
water box	−0.05 ± 0.03	−0.01 ± 0.02	8.48 ± 0.02	16.78 ± 0.04

[a] δ is R_2N−C−N−H dihedral angle. θ is the torsion improper centered on the secondary amine nitrogen. τ is the mean twisting angle between the C−N bond. χ_N is the out-of-plane bending angle, a measure of the degree of pyramidalization at the N atom. The standard errors of the mean are reported. Angles are expressed in degrees.

The population of the δ angle peaked around −6° while in solution was centered on 0°. The different behavior of the ligand within the enzyme and in solution can be appreciated by looking at the population of δ and θ in Figure 4. The distribution for **2** in complex with FAAH was centered around θ values of 5−6°. In solution, the maximum of the distribution for θ values was centered on zero, which indicated that the most abundant population of conformers was characterized by the planarity of the amide bond. Average values obtained for the Dunitz τ and χ_N angles are here reported for completeness. Within the enzyme, τ was 11.16 ± 0.02° and the nitrogen was partially pyramidalized with an average χ_N value of 22.74 ± 0.04°. In solution, the average τ and χ_N angles were 8.48 ± 0.02° and 16.78 ± 0.04°, respectively. This further indicated that the amide functional group was more distorted when it was simulated in complex with the enzyme, compared to its behavior in solution. Structural data are reported in Table 2.

*(h/r) FAAH·Cpd3 (****3****) Complex*. The MD simulations conducted with the inactive compound displayed an rmsd for the whole protein of 2.33 ± 0.19 Å, while the rmsd was 1.45 ± 0.12 Å for only the heavy atoms. The rmsd of **3** was 1.36 ± 0.41 Å, while

dx.doi.org/10.1021/jm2004283 |*J. Med. Chem.* 2011, 54, 6612–6623

the urea functional group was shown to be very stable (rmsd = 0.09 ± 0.03 Å). The carbamoylation distance was equal to 3.72 ± 0.19 Å, which was remarkably larger than that found for the active compounds. In addition, we observed the breaking of the catalytic triad H-bond network. In fact, the Ser241−Ser217 distance was ∼3.78 ± 0.36 Å, while the length of the H-bond between Ser217 and Lys142 increased to a value of 3.14 ± 0.91 Å during the simulations. Actually, along the simulations, **3** moved away from Ser241, inducing an increase in the carbamoylation distance. This occurred at different times in the two monomers: after ∼2−3 ns in Mnr B and within the first picoseconds of dynamics in Mnr A (see the Supporting Information for further details). Overall, **3** did not retain the starting interactions between its carbonyl oxygen and the FAAH oxyanion hole during the simulations, thus making useless any further investigation via QM/MM calculations. Moreover, in contrast to what was observed with the active compounds, it was not possible to detect a stable H-bond interaction between the hydrogen atoms of the urea functional group and the main chain carbonyl oxygen of the enzymatic Met191.

Amide Bond in ***3***. The urea functionality conserved a planar geometry both in FAAH and in solution. Indeed, the δ angle displayed similar values within FAAH and in solution ($\delta_{FAAH} = -1.31 \pm 0.03°$; $\delta_{water\ box} = -0.05 \pm 0.03°$). Likewise, θ assumed values equal to 1.59 ± 0.02° within the enzyme and 0.03 ± 0.02° in water. In fact, no correlation was observed between the δ and θ angles (see the δ vs θ correlation plot in Figure 6).

δ and θ distributions were centered on zero, when simulated in FAAH and in solution (Figure 4). As expected, the τ and χ_N angles showed comparable values in FAAH and in water. The average τ angle was ∼8.20 ± 0.01° in FAAH and ∼8.41 ± 0.02° in water. The average χ_N was 16.68 ± 0.08° in FAAH and 16.64 ± 0.04° in water. Other relevant geometrical parameters are listed in Table 3. Overall, the urea geometry was quite rigid and planar, both within FAAH and in solution, indicating that FAAH was not able to induce the distortion of the amide bond in **3**.

QM/MM Calculations. The nucleophilic attack on a carbonyl carbon can be described by the Fukui frontier molecular orbital theory.[36] Accordingly, the reaction occurs when the highest occupied bonding molecular orbital (HOMO) of the nuclephile overlaps the lowest unoccupied antibonding molecular orbital (LUMO) of the electrophilic species. Along the reaction coordinate, the HOMO−LUMO gap becomes narrower and favors reactivity. In this study, the hydroxyl oxygen of the catalytic Ser241 is the nucleophile that transfers electrons from its HOMO to the LUMO of the substrate (i.e., the carbonyl carbon of the ligand). We calculated the $\Delta E_{LUMO-HOMO}$ over the range of conformations of the amide bond and the average $\Delta E_{LUMO-HOMO}$ obtained for distorted and planar conformations, for both FAAH·**1** and FAAH·**2** complexes, as described in Computational Materials and Methods.

The most distorted conformations ($-40° < \delta < -35°$) showed $\Delta E_{LUMO-HOMO}$ values of ∼8.50 eV for the FAAH·**1** complex and ∼9.50 eV for the FAAH·**2** complex (Figure 7). When the δ angle was close to 0° (i.e., planar conformations), the $\Delta E_{LUMO-HOMO}$ became gradually larger and reached values of 10.27 eV for the FAAH·**1** complex and 10.25 eV for the FAAH·**2** complex. The $\Delta E_{LUMO-HOMO}$ trend, from distorted to planar conformations, is easily seen in Figure 7, which highlights a smaller gap for distorted conformations (i.e., high reactivity toward amide bond hydrolysis).

Centering the analysis on complexes showing a distorted C−N bond (see Computational Materials and Methods), we found the average $\Delta E_{LUMO-HOMO}$ was 9.33 ± 0.18 eV for **1**, while the analogue complexes characterized by a planar amide bond had a $\Delta E_{LUMO-HOMO}$ of 9.73 ± 0.18 eV, resulting in a $\Delta\Delta E_{LUMO-HOMO}$ of 0.40 eV. For complexes in which **2** showed a distorted amide bond, the average $\Delta E_{LUMO-HOMO}$ was equal to 9.65 ± 0.24 eV. In this case, the planar analogues showed an average $\Delta E_{LUMO-HOMO}$ of 10.02 ± 0.25 eV, resulting in a $\Delta\Delta E_{LUMO-HOMO}$ of 0.37 eV.

The localization of the frontier orbitals was also analyzed. For the FAAH·**1** complex, the LUMO of the distorted amide was

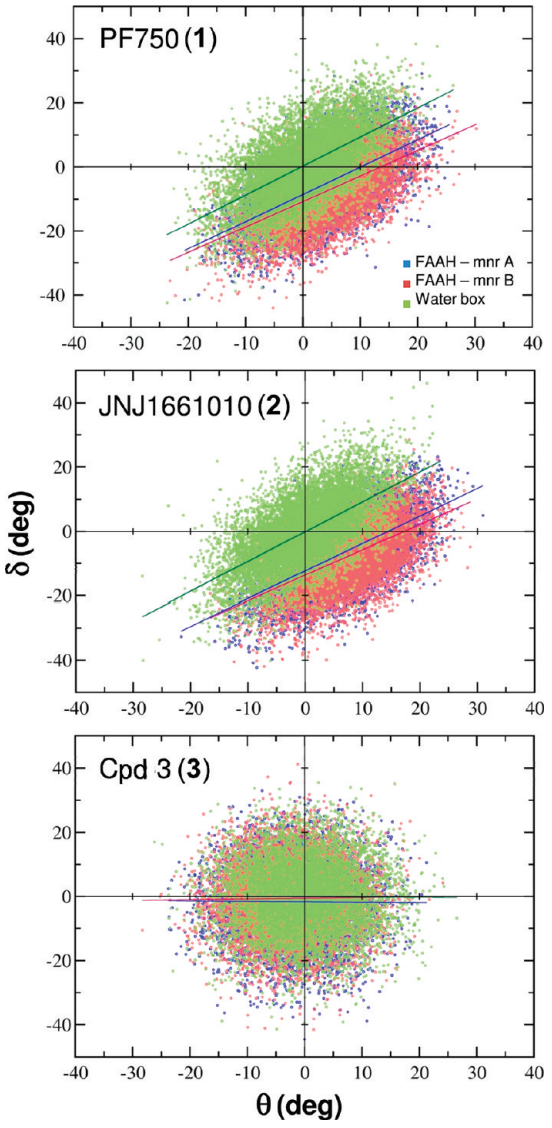

Figure 6. Correlation diagrams between δ and θ angles for **1**−**3** in complex with FAAH and in water. The δ vs θ correlation line is colored blue (Mnr A) or red (Mnr B). In solution, the δ vs θ correlation line is colored green. For **1**, the δ and θ angles are linearly correlated both in FAAH and in solution ($R_{FAAH}^2 = 0.60$; $R_{H_2O}^2 = 0.60$). The δ vs θ regression lines are distinctly shifted with respect to those in solution: within FAAH the *y*-intercept is approximately −9.7°, while in solution, the *y*-intercept crosses the axis origin (∼0.3°). This further indicates the structural deformation of the amide bond of the inhibitor in complex with FAAH. For **2**, the δ and θ angles are linearly correlated ($R_{FAAH}^2 = 0.59$; $R_{H_2O}^2 = 0.62$). The *y*-intercept is approximately −13.1°, while it is approximately −0.1° in water. For **3**, there is no correlation between the δ and θ angles.

Table 3. Average over the Last ~98 ns of MD Simulation for Inhibitor 3 within FAAH and in Solution[a]

	δ	θ	τ	χ_N
Mnr A	1.31 ± 0.03	1.53 ± 0.03	8.18 ± 0.02	16.62 ± 0.04
Mnr B	1.30 ± 0.03	1.63 ± 0.02	8.22 ± 0.02	16.74 ± 0.04
FAAH	1.31 ± 0.03	1.59 ± 0.02	8.20 ± 0.01	16.68 ± 0.03
water box	−0.05 ± 0.03	0.03 ± 0.02	8.41 ± 0.02	16.64 ± 0.04

[a] δ is the $R_2N-C-N-H$ dihedral angle. θ is the torsion improper centered on the secondary amine nitrogen. τ is the mean twisting angle between the C−N bond. χ_N is the out-of-plane bending angle, a measure of the degree of pyramidalization at the N atom. The standard errors of the mean are reported. Angles are expressed in degrees.

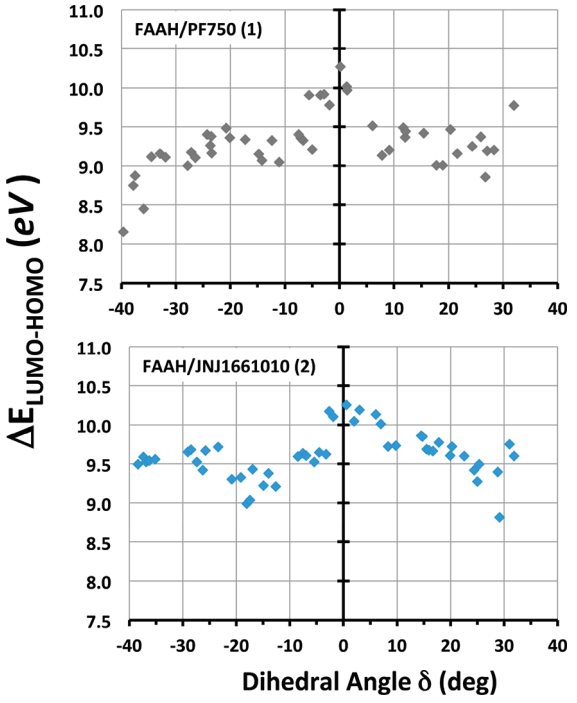

Figure 7. $\Delta E_{LUMO-HOMO}$ plotted vs dihedral angle δ for the FAAH·**1** (top) and FAAH·**2** (bottom) complexes. Fifty structures equally distributed over the δ range (−40° to 35°) were considered for each complex.

well localized on the **1** carbonyl, being turned toward the HOMO of the Ser241 nucleophile. On the other hand, the LUMO of the planar analogue was more delocalized and thus less prone to receiving electrons from the HOMO electron donor of Ser241 (Figure 8). The FAAH·**2** complex showed a similar topology of frontier orbital shape (Figure 8).

Overall, the QM/MM calculations showed a decreased $\Delta E_{LUMO-HOMO}$ for the protein·ligand complexes with a distorted amide bond with respect to the planar analogues. These data reflect a greater reactivity of the distorted amides toward nucleophilic attack.

DISCUSSION

Our results indicate that, within FAAH's binding site, the piperidine and piperazine inhibitors assume a specific conformation, which is characterized by a twist of the amide bond and partial pyramidalization at the amide bond nitrogen. Importantly,

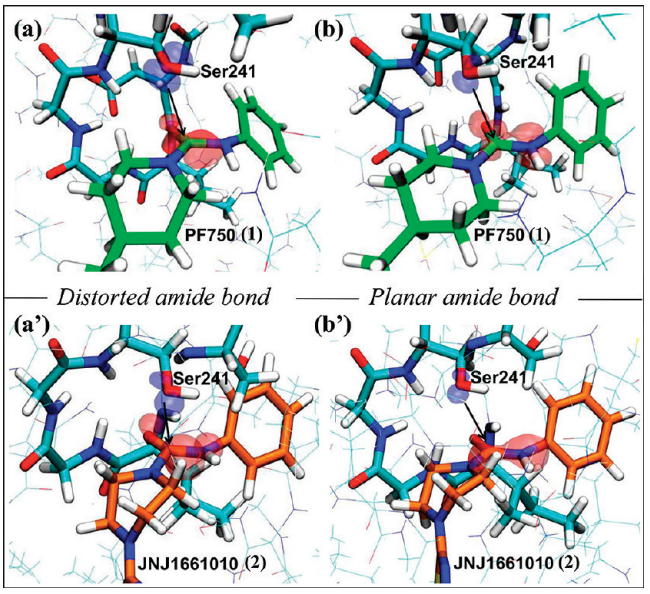

Figure 8. Shape of the frontier orbitals for the FAAH·**1** (top) and FAAH·**2** (bottom) complexes. Two representative snapshots characterized by distorted (a and a′) and planar (b and b′) amide bonds are shown for **1** and **2**, respectively. FAAH residues Ile238, Gly239, Gly240, Ser241, and Ser217 are colored cyan; **1** is colored green, and **2** is colored orange. The HOMO orbital of the Ser241 nucleophile is colored blue, while the LUMO orbital of the electrophile (i.e., the **1** and **2** carbonyl) is colored red.

this result can be used as a simple indication of the propensity of new urea-based compounds to act as a covalent inhibitor of FAAH.

The enzyme-induced distortion of the amide bond is evidenced by the δ and θ distribution curves of the piperidine and piperazine compounds bound to FAAH (Figure 4). Indeed, the amide bond of the inhibitors is planar when simulated in solution, as expected for force field-based simulations of this functional group, while it is distorted when simulated in complex with the enzyme FAAH (Figures 3 and 5).

As suggested by Greenberg,[20] the amide bond distortion increases the sp^3 character and the basicity of the amide nitrogen, making it available for protonation and coordination. As a consequence, distorted amides undergo nucleophilic attack more easily, compared to their planar analogues, as shown also by several informative computational studies.[37] Moreover, recent DFT studies[38] have shown that twisted amides, under different pH and solvent conditions, show a considerable acceleration of the hydrolysis compared to planar analogues. Also, kinetic experiments have demonstrated a significant acceleration for the hydrolysis of strained cyclic amides with a distorted amide bond,[39] such as the alkaline hydrolysis of the benzoquinuclidine-2-one, which is 10^7 times faster than its strain-free counterpart.[40] A final example is the highly twisted amide, 1-aza-2-adamantanone, which is exceedingly reactive toward hydrolysis under neutral conditions (at least 10^{10} times faster than a typical amide).[41] These arguments support the hypothesis that FAAH-induced distortion of the amide bond of the piperidine and piperazine FAAH inhibitors, evidenced by our simulations, could make the amide functional group more susceptible to nucleophilic attack by Ser241.[18] In other words, the amide distortion, which weakens the conjugation of the nitrogen lone pair with the

dx.doi.org/10.1021/jm2004283 |J. Med. Chem. 2011, 54, 6612–6623

carbonyl, could lead to a more efficient hydrolysis of the amide bond. This would explain the inhibitory activity of piperidine and piperazine compounds via their prompt formation of a covalent bond with Ser241 of FAAH. Furthermore, the increased basicity of the distorted amide could promote an easy protonation and release of the aniline leaving group during the reaction. QM/MM simulations are in progress to quantify the effect of the amide bond distortion in facilitating the reaction and formation of a covalent enzyme−inhibitor adduct in FAAH's catalytic site.

We calculated the free energy difference between the planar and most populated distorted amide conformations, according to the Boltzmann law of distribution. This difference turned out to be as small as ∼1 kcal/mol, in agreement with the force field potential for such a slight amide bond distortion (see the Supporting Information). Such a small gap between the planar and distorted conformations of the amide bond indicates an easy interchange between the two states. However, we observed a statistically relevant shift of the populated states of the ligand conformations toward distorted ones when in complex with FAAH, which favors inhibitor hydrolysis (Figure 4). Our QM/MM calculations suggested indeed a higher reactivity of the distorted amides toward nucleophilic attack, relative to those of their planar analogues. We detected a lower $\Delta E_{LUMO-HOMO}$ (9.33 ± 0.18 eV for **1** and 9.65 ± 0.24 eV for **2**) for distorted conformations, with respect to the planar analogues for which we found a larger $\Delta E_{LUMO-HOMO}$ (9.73 ± 0.18 eV for **1** and 10.02 ± 0.25 eV for **2**).

We speculate that the amide bond distortion could be primarily caused by the FAAH oxyanion hole residues (Ile238, Gly239, Gly240, and Ser241), which chelate the carbonyl oxygen of the cyclic inhibitors, while Met191 interacts with the ligand amide hydrogen (for detailed distances, see the Supporting Information). These simultaneous interactions that involve the urea functionality seem to be the major contribution to the twist of the amide bond in the piperidine and piperazine inhibitors. The peptide NH groups of the FAAH oxyanion hole draw electron density away from the urea functionality, while the Met191 H-bonds to the hydrogen of the ligand leaving group, weakening the amide bond. Furthermore, the heterocyclic moiety of the piperidine and piperazine inhibitors is closely surrounded by the Phe244, Tyr194, Ser193, Phe192, Val491, Ser193, Gly239, Gly216, Ser241, and Met191 residues. In this way, the enzyme generates a steric tension on the cyclic moiety of the inhibitor that enforces the deformation of the amide bond. It follows that the conformational flexibility of the piperidine and piperazine cycle appears to be critical for the activation of the urea-based FAAH*i* toward nucleophilic attack. The recent discovery of the piperidine and piperazine carbamates as efficacious inhibitors of the endocannabinoid hydrolases[42] emphasizes the effectiveness of the piperidine and piperazine structural motif for generating new covalent inhibitors of FAAH. Conversely, the inactive **3** is unable to establish favorable interactions with the FAAH oxyanion hole and shows a loss of binding. This, coupled to a lack of distortion of the amide bond, might explain the inability of **3** to inhibit FAAH.

Interestingly, the evidence of an enzyme-induced amide distortion reported herein can be related to other enzymes that are hypothesized to exploit the same mechanism to favor amide bond hydrolysis. For example, class A β-lactamases, which possess an oxyanion hole, are thought to induce a deformation of the sp^2 carbon of the endocyclic amide bond of the substrate β-lactam ring. This seems to be the major cause for β-lactam hydrolysis.[43] Also, in the case of carboxypeptidase Y, it was suggested that distortion of the peptide bond within the substrate may be crucial for hydrolytic activity.[44] In the case of the aspartic proteases, it was suggested that enzyme-induced distortion of the substrate amide could favor the attack of water on the polarized carbonyl.[45] Later, X-ray data for the aspartic proteinase endothiapepsin in complex with a potent difluorostatone-containing tripeptide renin confirmed this hypothesis.[46] In the process of protein splicing, X-ray and NMR experiments have suggested that the loss of amide planarity could facilitate the catalytic mechanism, by destabilizing the scissile amide bond.[47] Finally, a recent X-ray structure of the matrix metalloproteinase MMP-8 in complex with an *N*-hydroxyurea inhibitor showed a highly out-of-plane distortion of the amide bond, which undergoes hydrolysis.[48] In this scenario, our findings further clarify, with unprecedented detail, how the enzyme can induce specific conformations of the amide bond to facilitate its hydrolysis.

CONCLUSIONS

We have presented a comparative MD and QM/MM study to rationalize the mechanism used by the piperidine and piperazine urea-based compounds to inhibit FAAH. Three compounds were considered: two potent lead molecules, namely, piperidine **1** and piperazine **2**, and the inactive **3**. The structural flexibility of these compounds was analyzed either when in complex with FAAH or when in water.

MD simulations revealed a distortion of the amide bond of the piperidine and piperazine urea-based inhibitors when in complex with FAAH. This enzyme-induced conformational change may be a key step for FAAH inhibition. In fact, the linear inactive urea-based **3** does not show persistent deformations of the amide bond.

QM/MM calculations were used to evaluate the energy difference between the HOMO and LUMO orbitals ($\Delta E_{LUMO-HOMO}$). Results confirmed that distorted amides are more reactive toward the nucleophilic attack, in comparison to planar conformation. This further indicates that the enzyme-induced distortion facilitates amide hydrolysis.

Overall, our work corroborates the hypothesis[18] that the inhibitory activity of the piperidine and piperazine aryl ureas originates from their flexibility. The results show indeed that FAAH is able to induce a distortion of the amide bond of piperidine and piperazine inhibitors, which prompts the formation a covalent enzyme−inhibitor adduct. In other words, we provide a simple receipt for evaluating the propensity of new urea-based compounds to act as covalent inhibitors. Therefore, we believe these findings could be used for the rational design of more potent inhibitors bearing a cyclic urea-based moiety more prone to distortion of the amide bond.

ASSOCIATED CONTENT

Supporting Information. Further MD analysis and RESP charges, docking details for **2**, and further QM characterization of amide bond distortion. This material is available free of charge via the Internet at http://pubs.acs.org.

AUTHOR INFORMATION

Corresponding Authors

*E-mail: marco.devivo@iit.it Tel: +39 010 71781577. Fax: +39 010 7170187. (M.D.V.) or andrea.cavalli@unibo.it

Tel: +39 051 2099735 in Bologna. Tel: +39 010 71781530 in Genoa. Fax: +39 010 7170187. (A.C.).

■ ACKNOWLEDGMENT

We thank CINECA [centre for high performance computing, Bologna (IT)] and the Italian Institute of Technology computational platform initiative for providing computer time.

■ ABBREVIATIONS USED

AEA, anandamide; Mnr A, monomer A; Mnr B, monomer B; $\Delta E_{LUMO-HOMO}$, HOMO−LUMO energy gap; FAAH, fatty acid amide hydrolase; (*h*/*r*) FAAH, humanized rat FAAH protein; FAAH*i*, FAAH inhibitors; PEA, palmitoylethanolamide

■ REFERENCES

(1) Singh, J.; Petter, R. C.; Baillie, T. A.; Whitty, A. The resurgence of covalent drugs. *Nat. Rev. Drug Discovery* **2011**, *10* (4), 307–317.

(2) Potashman, M. H.; Duggan, M. E. Covalent modifiers: An orthogonal approach to drug design. *J. Med. Chem.* **2009**, *52* (5), 1231–1246.

(3) Ahn, K.; Johnson, D. S.; Cravatt, B. F. Fatty acid amide hydrolase as a potential therapeutic target for the treatment of pain and CNS disorders. *Expert Opin. Drug Discovery* **2009**, *4* (7), 763–784.

(4) (a) Desarnaud, F.; Cadas, H.; Piomelli, D. Anandamide amidohydrolase activity in rat brain microsomes. Identification and partial characterization. *J. Biol. Chem.* **1995**, *270* (11), 6030–6035. (b) Cravatt, B. F.; Giang, D. K.; Mayfield, S. P.; Boger, D. L.; Lerner, R. A.; Gilula, N. B. Molecular characterization of an enzyme that degrades neuromodulatory fatty-acid amides. *Nature* **1996**, *384* (6604), 83–87.

(5) (a) Lambert, D. M.; Vandevoorde, S.; Jonsson, K. O.; Fowler, C. J. The palmitoylethanolamide family: A new class of anti-inflammatory agents? *Curr Med. Chem.* **2002**, *9* (6), 663–674. (b) Devane, W. A.; Hanus, L.; Breuer, A.; Pertwee, R. G.; Stevenson, L. A.; Griffin, G.; Gibson, D.; Mandelbaum, A.; Etinger, A.; Mechoulam, R. Isolation and structure of a brain constituent that binds to the cannabinoid receptor. *Science* **1992**, *258* (5090), 1946–1949. (c) Rodriguez de Fonseca, F.; Navarro, M.; Gomez, R.; Escuredo, L.; Nava, F.; Fu, J.; Murillo-Rodriguez, E.; Giuffrida, A.; LoVerme, J.; Gaetani, S.; Kathuria, S.; Gall, C.; Piomelli, D. An anorexic lipid mediator regulated by feeding. *Nature* **2001**, *414* (6860), 209–212.

(6) Cravatt, B. F.; Demarest, K.; Patricelli, M. P.; Bracey, M. H.; Giang, D. K.; Martin, B. R.; Lichtman, A. H. Supersensitivity to anandamide and enhanced endogenous cannabinoid signaling in mice lacking fatty acid amide hydrolase. *Proc. Natl. Acad. Sci. U.S.A.* **2001**, *98* (16), 9371–9376.

(7) (a) Lichtman, A. H.; Shelton, C. C.; Advani, T.; Cravatt, B. F. Mice lacking fatty acid amide hydrolase exhibit a cannabinoid receptor-mediated phenotypic hypoalgesia. *Pain* **2004**, *109* (3), 319–327. (b) Gaetani, S.; Dipasquale, P.; Romano, A.; Righetti, L.; Cassano, T.; Piomelli, D.; Cuomo, V. The endocannabinoid system as a target for novel anxiolytic and antidepressant drugs. *Int. Rev. Neurobiol.* **2009**, *85*, 57–72. (c) Gobbi, G.; Bambico, F. R.; Mangieri, R.; Bortolato, M.; Campolongo, P.; Solinas, M.; Cassano, T.; Morgese, M. G.; Debonnel, G.; Duranti, A.; Tontini, A.; Tarzia, G.; Mor, M.; Trezza, V.; Goldberg, S. R.; Cuomo, V.; Piomelli, D. Antidepressant-like activity and modulation of brain monoaminergic transmission by blockade of anandamide hydrolysis. *Proc. Natl. Acad. Sci. U.S.A.* **2005**, *102* (51), 18620–18625.

(8) (a) Kathuria, S.; Gaetani, S.; Fegley, D.; Valino, F.; Duranti, A.; Tontini, A.; Mor, M.; Tarzia, G.; La Rana, G.; Calignano, A.; Giustino, A.; Tattoli, M.; Palmery, M.; Cuomo, V.; Piomelli, D. Modulation of anxiety through blockade of anandamide hydrolysis. *Nat. Med.* **2003**, *9* (1), 76–81. (b) Piomelli, D. The molecular logic of endocannabinoid signalling. *Nat. Rev. Neurosci.* **2003**, *4* (11), 873–884.

(9) (a) Ahn, K.; McKinney, M. K.; Cravatt, B. F. Enzymatic pathways that regulate endocannabinoid signaling in the nervous system. *Chem. Rev.* **2008**, *108* (5), 1687–1707. (b) McKinney, M. K.; Cravatt, B. F. Structure and function of fatty acid amide hydrolase. *Annu. Rev. Biochem.* **2005**, *74*, 411–432.

(10) (a) Bracey, M. H.; Hanson, M. A.; Masuda, K. R.; Stevens, R. C.; Cravatt, B. F. Structural adaptations in a membrane enzyme that terminates endocannabinoid signaling. *Science* **2002**, *298* (5599), 1793–1796. (b) Mileni, M.; Johnson, D. S.; Wang, Z.; Everdeen, D. S.; Liimatta, M.; Pabst, B.; Bhattacharya, K.; Nugent, R. A.; Kamtekar, S.; Cravatt, B. F.; Ahn, K.; Stevens, R. C. Structure-guided inhibitor design for human FAAH by interspecies active site conversion. *Proc. Natl. Acad. Sci. U.S.A.* **2008**, *105* (35), 12820–12824. (c) Mileni, M.; Kamtekar, S.; Wood, D. C.; Benson, T. E.; Cravatt, B. F.; Stevens, R. C. Crystal structure of fatty acid amide hydrolase bound to the carbamate inhibitor URB597: Discovery of a deacylating water molecule and insight into enzyme inactivation. *J. Mol. Biol.* **2010**, *400* (4), 743–754.

(11) (a) Guimaraes, C. R.; Boger, D. L.; Jorgensen, W. L. Elucidation of fatty acid amide hydrolase inhibition by potent α-ketoheterocycle derivatives from Monte Carlo simulations. *J. Am. Chem. Soc.* **2005** *127* (49), 17377–17384. (b) Lodola, A.; Mor, M.; Hermann, J. C.; Tarzia, G.; Piomelli, D.; Mulholland, A. J. QM/MM modelling of oleamide hydrolysis in fatty acid amide hydrolase (FAAH) reveals a new mechanism of nucleophile activation. *Chem. Commun.* **2005**, *35*, 4399–4401. (c) Lodola, A.; Mor, M.; Rivara, S.; Christov, C.; Tarzia, G.; Piomelli, D.; Mulholland, A. J. Identification of productive inhibitor binding orientation in fatty acid amide hydrolase (FAAH) by QM/MM mechanistic modelling. *Chem. Commun.* **2008**, 214–216. (d) Lodola, A.; Mor, M.; Sirirak, J.; Mulholland, A. J. Insights into the mechanism and inhibition of fatty acid amide hydrolase from quantum mechanics/molecular mechanics (QM/MM) modelling. *Biochem. Soc. Trans.* **2009**, *37* (Part 2), 363–367. (e) Tubert-Brohman, I.; Acevedo, O.; Jorgensen, W. L. Elucidation of hydrolysis mechanisms for fatty acid amide hydrolase and its Lys142Ala variant via QM/MM simulations. *J. Am. Chem. Soc.* **2006**, *128* (51), 16904–16913.

(12) Seierstad, M.; Breitenbucher, J. G. Discovery and development of fatty acid amide hydrolase (FAAH) inhibitors. *J. Med. Chem.* **2008**, *51* (23), 7327–7343.

(13) Tarzia, G.; Duranti, A.; Tontini, A.; Piersanti, G.; Mor, M.; Rivara, S.; Plazzi, P. V.; Park, C.; Kathuria, S.; Piomelli, D. Design, synthesis, and structure-activity relationships of alkylcarbamic acid aryl esters, a new class of fatty acid amide hydrolase inhibitors. *J. Med. Chem.* **2003**, *46* (12), 2352–2360.

(14) Mor, M.; Rivara, S.; Lodola, A.; Plazzi, P. V.; Tarzia, G.; Duranti, A.; Tontini, A.; Piersanti, G.; Kathuria, S.; Piomelli, D. Cyclohexylcarbamic acid 3′- or 4′-substituted biphenyl-3-yl esters as fatty acid amide hydrolase inhibitors: synthesis, quantitative structure-activity relationships, and molecular modeling studies. *J. Med. Chem.* **2004**, *47* (21), 4998–5008.

(15) (a) Clapper, J. R.; Duranti, A.; Tontini, A.; Mor, M.; Tarzia, G.; Piomelli, D. The fatty-acid amide hydrolase inhibitor URB597 does not affect triacylglycerol hydrolysis in rat tissues. *Pharmacol. Res.* **2006**, *54* (5), 341–344. (b) Piomelli, D.; Tarzia, G.; Duranti, A.; Tontini, A.; Mor, M.; Compton, T. R.; Dasse, O.; Monaghan, E. P.; Parrott, J. A.; Putman, D. Pharmacological profile of the selective FAAH inhibitor KDS-4103 (URB597). *CNS Drug Rev.* **2006**, *12* (1), 21–38.

(16) Clapper, J. R.; Moreno-Sanz, G.; Russo, R.; Guijarro, A.; Vacondio, F.; Duranti, A.; Tontini, A.; Sanchini, S.; Sciolino, N. R.; Spradley, J. M.; Hohmann, A. G.; Calignano, A.; Mor, M.; Tarzia, G.; Piomelli, D. Anandamide suppresses pain initiation through a peripheral endocannabinoid mechanism. *Nat. Neurosci.* **2010**, *13* (10), 1265–1270.

(17) Sit, S. Y.; Conway, C.; Bertekap, R.; Xie, K.; Bourin, C.; Burris, K.; Deng, H. Novel inhibitors of fatty acid amide hydrolase. *Bioorg. Med. Chem. Lett.* **2007**, *17* (12), 3287–3291.

(18) Ahn, K.; Johnson, D. S.; Fitzgerald, L. R.; Liimatta, M.; Arendse, A.; Stevenson, T.; Lund, E. T.; Nugent, R. A.; Nomanbhoy, T. K.; Alexander, J. P.; Cravatt, B. F. Novel mechanistic class of fatty acid amide hydrolase inhibitors with remarkable selectivity. *Biochemistry* **2007**, *46* (45), 13019–13030.

(19) Keith, J. M.; Apodaca, R.; Xiao, W.; Seierstad, M.; Pattabiraman, K.; Wu, J.; Webb, M.; Karbarz, M. J.; Brown, S.; Wilson, S.; Scott, B.; Tham, C. S.; Luo, L.; Palmer, J.; Wennerholm, M.; Chaplan, S.;

Breitenbucher, J. G. Thiadiazolopiperazinyl ureas as inhibitors of fatty acid amide hydrolase. *Bioorg. Med. Chem. Lett.* **2008**, *18* (17), 4838–4843.

(20) Greenberg, A.; Breneman, C. M.; Liebman, J. F. *The Amide Linkage: Structural Significance in Chemistry, Biochemistry, and Materials Science*; Wiley: New York, 2000.

(21) Morris, G. M.; Goodsell, D. S.; Halliday, R. S.; Huey, R.; Hart, W. E.; Belew, R. K.; Olson, A. J. Automated docking using a Lamarckian genetic algorithm and and empirical binding free energy function. *J. Comput. Chem.* **1998**, *19*, 1639–1662.

(22) Jorgensen, W. L.; Chandrasekhar, J.; Madura, J. D.; Impey, R. W.; Klein, M. L. Comparison of simple potential functions for simulating liquid water. *J. Chem. Phys.* **1983**, *79*, 926–935.

(23) Cornell, W. D.; Cieplak, P.; Bayly, C. I.; Gould, I. R.; Merz, K. M.; Ferguson, D. M.; Spellmeyer, D. C.; Fox, T.; Caldwell, J. W.; Kollman, P. A. A second generation force field for the simulation of proteins, nucleic acids, and organic molecules. *J. Am. Chem. Soc.* **1995**, *117*, 5179–5197.

(24) Hornak, V.; Abel, R.; Okur, A.; Strockbine, B.; Roitberg, A.; Simmerling, C. Comparison of multiple Amber force fields and development of improved protein backbone parameters. *Proteins* **2006**, *65* (3), 712–725.

(25) Wang, J.; Wolf, R. M.; Caldwell, J. W.; Kollman, P. A.; Case, D. A. Development and testing of a general Amber force field. *J. Comput. Chem.* **2004**, *25* (9), 1157–1174.

(26) Bayly, C. I.; Cieplak, P.; Cornell, W. D.; Kollman, P. A. A well-behaved electrostatic potential based method using charge restraints for deriving atomic charges: The RESP model. *J. Phys. Chem.* **1993**, *97*, 10269–10280.

(27) Ryckaert, J. P.; Ciccotti, G.; Berendsen, H. J. C. Numerical integration of Cartesian equations of motion of a system with constraints: Molecular dynamics of N-alkanes. *J. Comput. Phys.* **1977**, *23* (3), 327–341.

(28) Phillips, J. C.; Braun, R.; Wang, W.; Gumbart, J.; Tajkhorshid, E.; Villa, E.; Chipot, C.; Skeel, R. D.; Kale, L.; Schulten, K. Scalable molecular dynamics with NAMD. *J. Comput. Chem.* **2005**, *26* (16), 1781–1802.

(29) Feller, S. E.; Zhang, Y.; Pastor, R. W.; Brooks, R. W. Constant pressure molecular dynamics simulation: The Langevin piston method. *J. Chem. Phys.* **1995**, *103*, 4613–4621.

(30) (a) Gilli, G.; Bertolasi, V.; Bellucci, F.; Ferretti, V. Stereochemistry of the $R_1(X{=})C(sp^2){-}N(sp^3)R_2R_3$ fragment. Mapping of the cis-trans isomerization path by rotation around the C-N bond from crystallographic structural data. *J. Am. Chem. Soc.* **1986**, *108*, 2420–2424. (b) Winkler, F. K.; Dunitz, J. D. The non-planar amide group. *J. Mol. Biol.* **1971**, *59* (1), 169–182.

(31) (a) Humbel, S.; Sieber, S.; Morokuma, K. The IMOMO method: Integration of different levels of molecular orbital approximations for geometry optimization of large systems: Test for n-butane conformation and SN2 reaction: RCL + Cl^-. *J. Chem. Phys.* **1996**, *105*, 1959–1967. (b) Svensson, M.; Humbel, S.; Froese, R. D. J.; Matsubara, T.; Sieber, S.; Morokuma, K. ONIOM: A multilayered integrated MO + MM method for geometry optimizations and single point energy predictions. A test for Diels–Alder reactions and $Pt(P(t\text{-}Bu)_3)_2 + H_2$ oxidative addition. *J. Phys. Chem.* **1996**, *100*, 19357–19363.

(32) Frisch, M. J.; Trucks, G. W.; Schlegel, H. B.; Scuseria, G. E.; Robb, M. A.; Cheeseman, J. R.; Scalmani, G.; Barone, V.; Mennucci, B.; Petersson, G. A.; Nakatsuji, H.; Caricato, M.; Li, X.; Hratchian, H. P.; Izmaylov, A. F.; Bloino, J.; Zheng, G.; Sonnenberg, J. L.; Hada, M.; Ehara, M.; Toyota, K.; Fukuda, R.; Hasegawa, J.; Ishida, M.; Nakajima, T.; Honda, Y.; Kitao, O.; Nakai, H.; Vreven, T.; Montgomery, J. J. A.; Peralta, J. E.; Ogliaro, F.; Bearpark, M.; Heyd, J. J.; Brothers, E.; Kudin, K. N.; Staroverov, V. N.; Kobayashi, R.; Normand, J.; Raghavachari, K.; Rendell, A.; Burant, J. C.; Iyengar, S. S.; Tomasi, J.; Cossi, M.; Rega, N.; Millam, N. J.; Klene, M.; Knox, J. E.; Cross, J. B.; Bakken, V.; Adamo, C.; Jaramillo, J.; Gomperts, R.; Stratmann, R. E.; Yazyev, O.; Austin, A. J.; Cammi, R.; Pomelli, C.; Ochterski, J. W.; Martin, R. L.; Morokuma, K.; Zakrzewski, V. G.; Voth, G. A.; Salvador, P.; Dannenberg, J. J.; Dapprich, S.; Daniels, A. D.; Farkas, Ö.; Foresman, J. B.; Ortiz, J. V.; Cioslowski, J.; Fox, D. J. *Gaussian 09*, revision A.1; Gaussian, Inc.: Wallingford, CT, 2009.

(33) Vreven, T.; Byun, K. S.; Komaromi, I.; Dapprich, S.; Montgomery, J. A.; Morokuma, K.; Frisch, M. J. Combining quantum mechanics methods with molecular mechanics methods in ONIOM. *J. Chem. Theory Comput.* **2006**, *2*, 815–826.

(34) Morrell, C.; Grand, A.; Toro-Labbé, A. New dual descriptor for chemical reactivity. *J. Phys. Chem. A* **2005**, *109*, 205–212.

(35) Johnson, D. S.; Ahn, K.; Kesten, S.; Lazerwith, S. E.; Song, Y.; Morris, M.; Fay, L.; Gregory, T.; Stiff, C.; Dunbar, J. B., Jr.; Liimatta, M.; Beidler, D.; Smith, S.; Nomanbhoy, T. K.; Cravatt, B. F. Benzothiophene piperazine and piperidine urea inhibitors of fatty acid amide hydrolase (FAAH). *Bioorg. Med. Chem. Lett.* **2009**, *19* (10), 2865–2869.

(36) Fukui, K. *Theory of Orientation and Stereoselection*; Springer-Verlag: New York, 1975.

(37) (a) Alexandrova, A. N.; Jorgensen, W. L. Why urea eliminates ammonia rather than hydrolyzes in aqueous solution. *J. Phys. Chem. B* **2007**, *111* (4), 720–730. (b) Blumberger, J.; Ensing, B.; Klein, M. L. Formamide hydrolysis in alkaline aqueous solution: Insight from ab initio metadynamics calculations. *Angew. Chem., Int. Ed.* **2006**, *45* (18), 2893–2897. (c) Bryantsev, V. S.; Firman, T. K.; Hay, B. P. Conformational analysis and rotational barriers of alkyl- and phenyl-substituted urea derivatives. *J. Phys. Chem. A* **2005**, *109* (5), 832–842. (d) Cascella, M.; Raugei, S.; Carloni, P. Formamide hydrolysis investigated by multiple-steering ab initio molecular dynamics. *J. Phys. Chem. B* **2004**, *108*, 369–375.

(38) (a) Lopez, X.; Mujika, J. I.; Blackburn, G. M.; Karplus, M. Alkaline hydrolysis of amide bonds: Effect of bond twist and nitrogen pyramidalization. *J. Phys. Chem. A* **2003**, *107*, 2304–2315. (b) Mujika, J. I.; Formoso, E.; Mercero, J. M.; Lopez, X. Reaction mechanism of the acidic hydrolysis of highly twisted amides: Rate acceleration caused by the twist of the amide bond. *J. Phys. Chem. B* **2006**, *110*, 15000–15011. (c) Mujika, J. I.; Mercero, J. M.; Lopez, X. A theoretical evaluation of the pKa for twisted amides using density functional theory and dielectric continuum methods. *J. Phys. Chem. A* **2003**, *107*, 6099–6107. (d) Mujika, J. I.; Mercero, J. M.; Lopez, X. Water-promoted hydrolysis of a highly twisted amide: Rate acceleration caused by the twist of the amide bond. *J. Am. Chem. Soc.* **2005**, *127*, 445–4453.

(39) Wang, Q. P.; Bennet, A. J.; Brown, R. S.; Santarsiero, B. D. Distorted amides as models for activated peptide N-C(O) units. 3. Synthesis, hydrolytic profile, and molecular structure of 2,3,4,5-tetrahydro-2-oxo-1,5-propanobenzazepine. *J. Am. Chem. Soc.* **1991**, *113*, 5757–5765.

(40) Blackburn, G. M.; Skaife, C. J.; Kay, I. T. Strain effects in acyl transfer reactions. Part 5. The kinetics of hydrolysis of benzoquinuclidin-2-one: A torsionally-distorted amide. *J. Chem. Res.* **1980**, 3650–3669.

(41) Kirby, A. J.; Komarov, I. V.; Feeder, N. Synthesis, structure and reactions of the most twisted amide. *J. Chem. Soc., Perkin Trans. 2* **2001**, 522–529.

(42) (a) Long, J. Z.; Jin, X.; Adibekian, A.; Li, W.; Cravatt, B. F. Characterization of tunable piperidine and piperazine carbamates as inhibitors of endocannabinoid hydrolases. *J. Med. Chem.* **2010**, *53* (4), 1830–1842. (b) Long, J. Z.; Nomura, D. K.; Vann, R. E.; Walentiny, D. M.; Booker, L.; Jin, X.; Burston, J. J.; Sim-Selley, L. J.; Lichtman, A. H.; Wiley, J. L.; Cravatt, B. F. Dual blockade of FAAH and MAGL identifies behavioral processes regulated by endocannabinoid crosstalk in vivo. *Proc. Natl. Acad. Sci. U.S.A.* **2009**, *106* (48), 20270–20275.

(43) (a) Dal Peraro, M.; Vila, A. J.; Carloni, P.; Klein, M. L. Role of zinc content on the catalytic efficiency of B1 metallo β-lactamases. *J. Am. Chem. Soc.* **2007**, *129* (10), 2808–2816. (b) Park, H.; Brothers, E. N.; Merz, K. M., Jr. Hybrid QM/MM and DFT investigations of the catalytic mechanism and inhibition of the dinuclear zinc metallo-β-lactamase CcrA from *Bacteroides fragilis*. *J. Am. Chem. Soc.* **2005**, *127* (12), 4232–4241.

(44) Stennicke, H. R.; Mortensen, U. H.; Breddam, K. Studies on the hydrolytic properties of (serine) carboxypeptidase Y. *Biochemistry* **1996**, *35* (22), 7131–7141.

(45) Pearl, L. H. The catalytic mechanism of aspartic proteinases. *FEBS Lett.* **1987**, *214* (1), 8–12.

(46) Veerapandian, B.; Cooper, J. B.; Sali, A.; Blundell, T. L.; Rosati, R. L.; Dominy, B. W.; Damon, D. B.; Hoover, D. J. Direct observation by X-ray analysis of the tetrahedral "intermediate" of aspartic proteinases. *Protein Sci.* **1992**, *1* (3), 322–328.

(47) (a) Poland, B. W.; Xu, M. Q.; Quiocho, F. A. Structural insights into the protein splicing mechanism of PI-SceI. *J. Biol. Chem.* **2000**, *275* (22), 16408–16413. (b) Romanelli, A.; Shekhtman, A.; Cowburn, D.; Muir, T. W. Semisynthesis of a segmental isotopically labeled protein splicing precursor: NMR evidence for an unusual peptide bond at the N-extein-intein junction. *Proc. Natl. Acad. Sci. U.S.A.* **2004**, *101* (17), 6397–6402.

(48) Campestre, C.; Agamennone, M.; Tortorella, P.; Preziuso, S.; Biasone, A.; Gavuzzo, E.; Pochetti, G.; Mazza, F.; Hiller, O.; Tschesche, H.; Consalvi, V.; Gallina, C. N-Hydroxyurea as zinc binding group in matrix metalloproteinase inhibition: Mode of binding in a complex with MMP-8. *Bioorg. Med. Chem. Lett.* **2006**, *16* (1), 20–24.